Phys Chem Minerals (2012) 39:789–795
DOI 10.1007/s00269-012-0533-9

ORIGINAL PAPER

Co_3O_4 nanoparticles on the surface of halloysite nanotubes

Yi Zhang · Huaming Yang

Received: 24 April 2012 / Accepted: 18 July 2012 / Published online: 31 July 2012

Abstract Co_3O_4 nanoparticles were successfully deposited on the surface of natural halloysite nanotubes (HNTs) to produce Co_3O_4/HNTs composites. The structure and morphology of the samples were characterized using X-ray diffraction, field-emission scanning electron microscope, transmission electron microscope and Fourier transform infrared. The results indicated that Co_3O_4 nanoparticles were uniformly attached on the surface of HNTs with narrow size distribution. Co_3O_4/HNTs exhibited an excellent photocatalytic efficiency for degradation of methyl blue under UV light, better than Co_3O_4 and HNTs mixture, HNTs and pure Co_3O_4. The mechanism of enhanced photocatalytic activity of Co_3O_4/HNTs was also proposed.

Keywords Halloysite nanotubes (HNTs) · Cobalt oxides · Surface deposition · Photodegradation

Introduction

Transition metal oxides have been considered as the promising active material candidates due to their unique and irreplaceable properties in optics (Liu and Aydil 2009), magnetism (Takada et al. 2001), catalysis (Cao et al. 2006) and electricity (Hu et al. 2008). The combination of active materials and ancillary materials to form functional systems had been highly expected to promote their functionalities and applications in many fields. Cobalt oxides have been widely used in glass industry for colored glasses and in chemical processes as a catalytic activator in oxidation reactions (Natile and Glisenti 2002; Hu et al. 2008; Casas-Cabanas et al. 2009; Jiao and Frei 2009; Artero et al. 2011; Liang et al. 2011; Yeo and Bell 2011). Also, there were some reports on the degradation of toxic gases like NO_x using Co_3O_4 (Wöllenstein et al. 2003; Li et al. 2010).

Carbon nanotubes (CNTs) have been used as support to assemble functional nanoparticles to produce novel nanocomposites, such as TiO_2 (Liu and Aydil 2009; Woan et al. 2009). As for the same active phase, it was noteworthy that CNTs-based materials often showed higher activity than the samples deposited on other supports like alumina, silica, or even activated carbon (Endo et al. 2008; Zhai et al. 2010). Halloysite ($Al_2Si_2O_5(OH)4{\cdot}2H_2O$) (Guimarães et al. 2010), a hydrated layered aluminosilicate of the kaolinite group, possesses hollow cylinders formed by multiply rolled layers containing octahedral gibbsite $Al(OH)_3$ and tetrahedral SiO_4 sheets (i.e., halloysite nanotubes, HNTs). Variable content of water molecules in the interlayer space of the halloysite structure affected the interplanar distance in the range from 0.7 nm (dehydrated form) to 1.0 nm (fully hydrated form). HNTs have been the subject of extensive researches, because they have, with respect to other minerals of kaolinite group, relatively higher specific surface area, porosity, as well as cation exchange capacity (Gualtieri 2001; Joussein et al. 2005; Hu and Yang 2012; Zhang and Yang 2012). Recently, HNTs presented exceptional physical properties that made them suitable for applications in different fields such as medicine (Levis and Deasy 2002; Lvov et al. 2008; Shchukin et al. 2008; Abdullayev et al. 2009; Veerabadran et al. 2009; Hughes and King 2010; Zhai et al. 2010), electronics, polymers (Du

Y. Zhang · H. Yang (✉)
School of Minerals Processing and Bioengineering, Central South University, Changsha 410083, China
e-mail: hmyang@csu.edu.cn

Y. Zhang · H. Yang
Research Center for Mineral Materials, Central South University, Changsha 410083, China

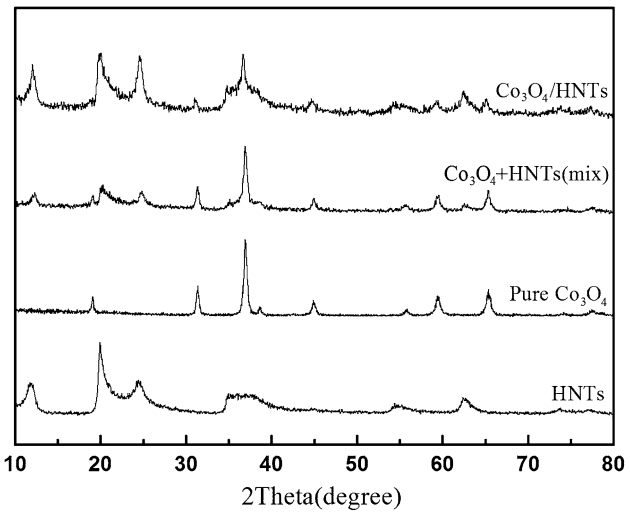

Fig. 1 XRD patterns of HNTs, pure Co_3O_4, Co_3O_4+HNTs(mix) and Co_3O_4/HNTs

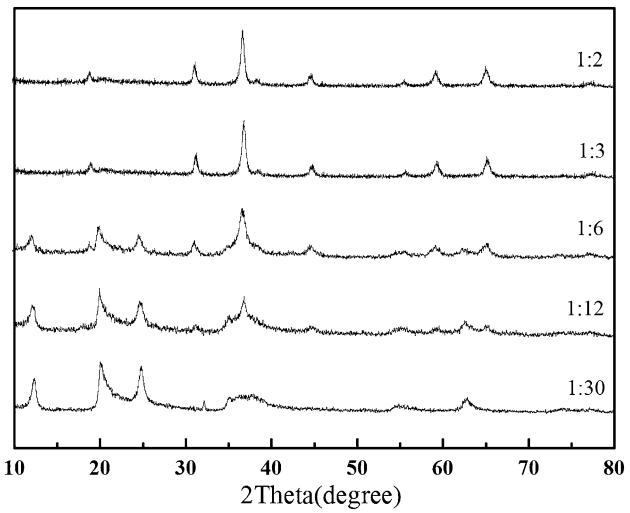

Fig. 2 XRD patterns of the Co_3O_4/HNTs with different Co_3O_4/HNTs mass ratios

et al. 2010) and catalysis (Du et al. 2010; Wang et al. 2011), but there are few reports to the best of our knowledge concerning the assembled Co_3O_4 on the surface of HNTs and its photocatalytic activity.

In this paper, we demonstrate a novel route to the synthesis of Co_3O_4/HNTs nanocomposites via assembling the Co_3O_4 nanoparticles on the outer surface of HNTs, which was called the incipient wetness impregnation (Delannoy et al. 2006; Azadi et al. 2010) based on the difference in the interface energies of organic and aqueous solutions with the HNTs surface.

Experimental

The halloysite nanotubes (HNTs), obtained from Hunan, China, was firstly dispersed and dried for 12 h at 80 °C.

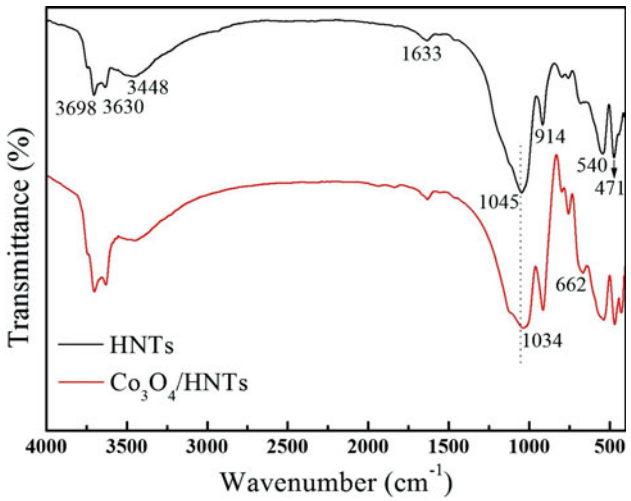

Fig. 3 FTIR spectra of HNTs and Co_3O_4/HNTs

All chemicals were analytical grade and used without further purification. Co_3O_4/HNTs nanocomposites were synthesized as follows: 500 mg of halloysite was mixed with 10 mL of ethylbenzene, ultrasonically treated for 10 min to form the HNTs slurry. In the second step, 50, 125, 250, 500 and 750 mg of cobalt acetate ($Co(AC)_2{\cdot}4H_2O$) were dissolved in 20 mL of distilled water according to the designed Co_3O_4/HNTs mass ratios (1:2, 1:3, 1:6, 1:12 and 1:30). The solution was then slowly added to 500 mg of above HNTs slurry using a Pasteur pipet, while continuously stirring the paste with a glass stick. The mixture was dried at 323 K for 10 h, subsequently heated in static air at 623 K for 3 h with a heating rate of 50 °C/min to finally form Co_3O_4/HNTs composites. For comparison, pure Co_3O_4 nanoparticles were prepared according to the above procedure without the addition of halloysite, and Co_3O_4+HNTs (mix) were also synthesized according to the above procedure without the addition of organic solvent.

The crystalline phases were identified by X-ray diffraction (XRD) analysis with a RIGAKU D/max-2550VB+ 18 kW powder diffractometer with Cu Kα-radiation ($\lambda = 1.5418$ Å). The data were collected from 10° to 80° of 2θ with a scanning speed in 2° min^{-1}. The crystal sizes (D) of cobalt oxides were estimated according to the Scherrer's equation: $D = 0.9\lambda/\beta\cos\theta$, where λ is the X-ray wavelength, β is the full width of the reflection at half height and θ is the diffraction angle. JSM-6700F field-emission scanning electron microscope (FESEM) and transmission electron microscope (TEM, JEOL IEM-200CX) equipped with an energy-dispersive X-ray spectrometer (EDAX) at an accelerating voltage of 200 kV were used in this analysis. Fourier transform infrared (FTIR) spectra were recorded on a Nicolet 5700 spectrophotometer using KBr pellets for samples. Photoluminescence (PL) spectra of the samples were recorded by Hitachi F-4500 under the excitation light at 254 nm.

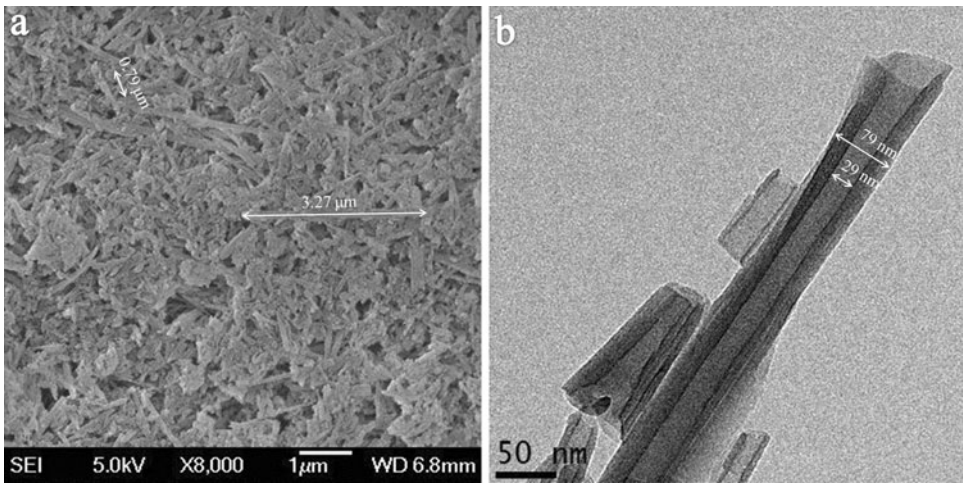

Fig. 4 **a** SEM and **b** TEM images of halloysite

The photocatalytic activity of Co_3O_4/HNTs was investigated according to the photodegradation of methyl blue (MB). The photodegradation experiments were carried out in a closed box. In each experiment, 50 mg of the sample was suspended in 250 mL of 200 mg/L MB aqueous solution. The temperature of the reactant solution was maintained below 288 K by a flow of cooling water. UV radiation source was a 60 W high-pressure mercury lamp. Absorbance variations of MB aqueous before and after photocatalysis for different times were measured on 756P spectrophotometer (Shanghai, China). The decolorization ratio of contaminant was calculated by the following formula: $D = (A_0 - A_t)/A_0 \times 100\ \%$; here, A_t is the absorbance of the contaminant solution at different reaction time t and A_0 is the initial MB solution.

Results and discussion

Figure 1 showed the XRD patterns of HNTs, pure Co_3O_4, Co_3O_4+HNTs(mix) and Co_3O_4/HNTs samples. For the HNTs sample, all of the observed diffraction lines were indexed to the characteristic of halloysite. However, three new diffraction lines at $2\theta = 44.8$, 59.4, 65.2 and a stronger diffraction line at $2\theta = 36.8$ can be observed. XRD patterns of pure Co_3O_4 and corresponding composites with HNTs all demonstrated the successful preparation of Co_3O_4 according to JCPDS 42-1467, but the XRD patterns of HNTs changed to some degree during the process. The diffraction lines became stronger with an increasing amount of Co_3O_4 (Fig. 2), and any other impurities were not detected. The crystal size of the Co_3O_4 nanoparticles calculated by the Scherrer's equation was 3–5 nm.

FTIR spectra of the HNTs and Co_3O_4/HNTs were used to investigate the composition and structure of the resultant samples. The Co_3O_4/HNTs possessed some obvious signals attributed to HNTs (Fig. 3), such as the deformations of Al–O–Si and Si–O–Si at 536 and 462 cm^{-1}, and two weak bands at 3,448 and 1,635 cm^{-1} were respectively attributed to the intercalated water and the surface –OH groups H-bonded to interlayer water. HNTs also exhibited two Al_2OH-stretching bands at 3,698 and 3,630 cm^{-1}, each –OH being linked to two Al atoms, and single Al_2OH–bending band at 914 cm^{-1}, respectively. Compared to HNTs, the IR spectrum of Co_3O_4/HNTs displayed a distinct band at 662 cm^{-1} originated from the stretching vibration of the metal–oxygen bonds, which was attributed to the ABO_3 vibration (A denoted the Co^{2+} in a tetrahedral hole). The Si–O broad stretching band around 1,034 cm^{-1} shifted to 1,045 cm^{-1}, indicating the existence of hydrogen bonding between Co_3O_4 and outer surfaces of HNTs. No other changes in the IR spectra of HNTs was observed.

The majority of the samples consisted of cylindrical tubes with 50–75 nm in diameter and 0.5–3 μm in length (Fig. 4). FESEM image revealed the empty lumen structure of HNTs with 15–30 nm in diameter (Fig. 4a), consistent with the corresponding TEM image (Fig. 4b). After loaded, a large amount of small Co_3O_4 nanoparticles were deposited on the surface of the HNTs (Fig. 5a), which made the surface of Co_3O_4/HNTs become more rough. The corresponding energy-dispersive X-ray spectrometry (EDX) indicated that Co_3O_4/HNTs composites were composed of the elements Al, Si, Co, and O (Fig. 5b), and the Cu peaks originated from the holey carbon-Cu grid. TEM and HRTEM images also demonstrated the location of the smaller Co_3O_4 nanoparticles on the whole external surface of HNTs (Fig. 5d).

Assembling nanoparticles outside the closed HNTs was a challenging task. The used organic solvent has a low surface tension, will remain inside the nanotubes but protect its inner surface from metal deposition. Here we selected ethylbenzene as organic solvent with high boiling point (409 K) and low solubility (1.6×10^{-2}). The two-step impregnation can be described was as follows (Fig. 6).

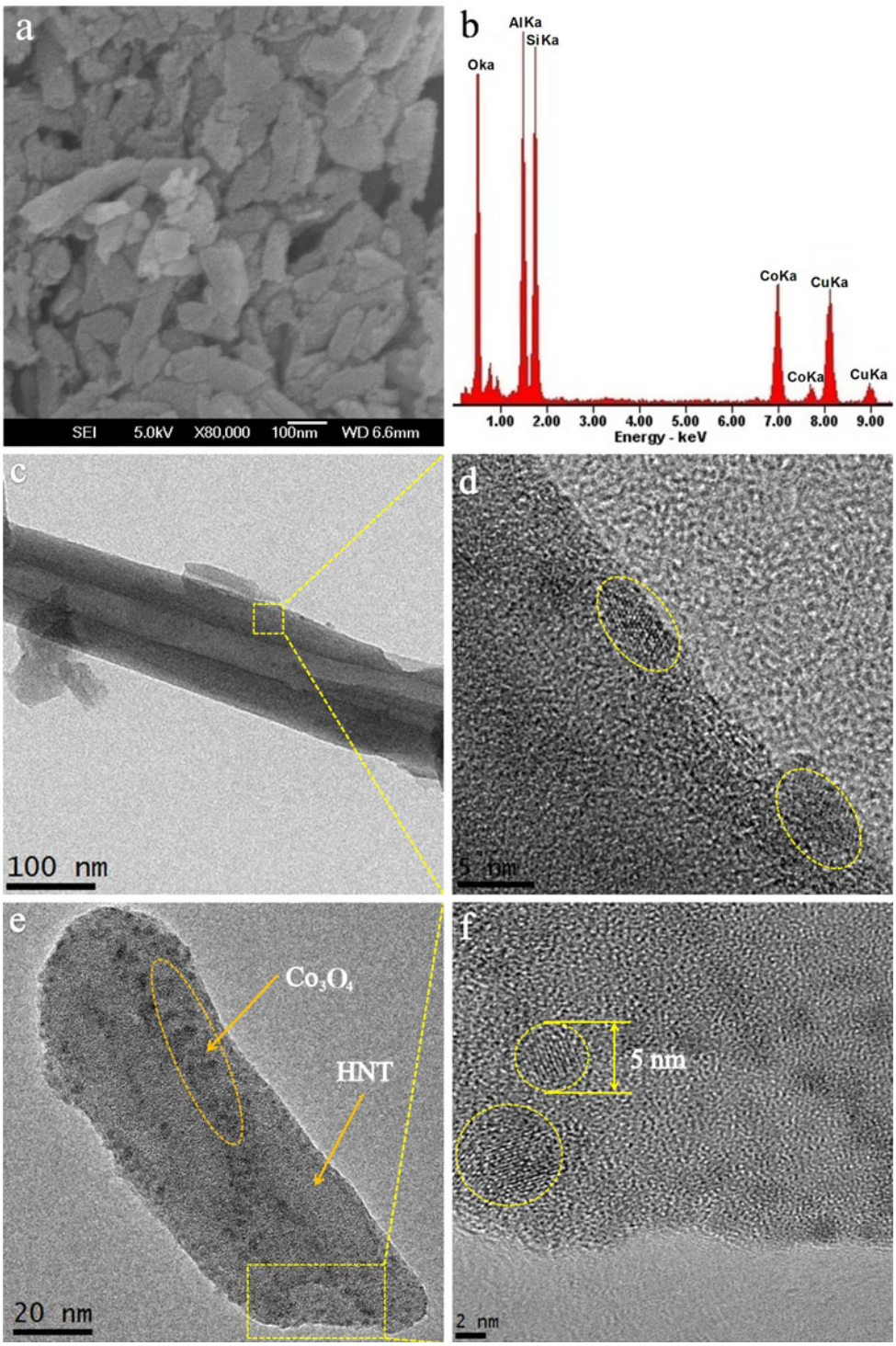

Fig. 5 **a** FESEM image of Co_3O_4/HNTs and **b** EDX spectrum of Co_3O_4 nanoparticles on the external surface of HNT, **c**, **e** TEM and **d**, **f** corresponding HRTEM images of Co_3O_4/HNTs

In the first step, we impregnated the HNTs with organic solvent, which will wet and fill the nanotubes easily. Organic solvent often had a high vapor pressure, and their evaporation was very fast; therefore, it was put in excess in order to ensure the complete filling of the HNTs and the protection of the inner tubes from metal deposition. Secondly, an aqueous solution containing the metal precursor was added, but could not penetrate the HNTs due to its higher liquid/solid interface energy. Thus, the inner remained protected and the nanoparticles deposition only happened on the outer surface.

The photocatalytic activities of Co_3O_4/HNTs, Co_3O_4+ HNTs (mix), Co_3O_4 and HNTs were shown in Fig. 7. Pure HNTs showed nearly no photocatalytic effect but an

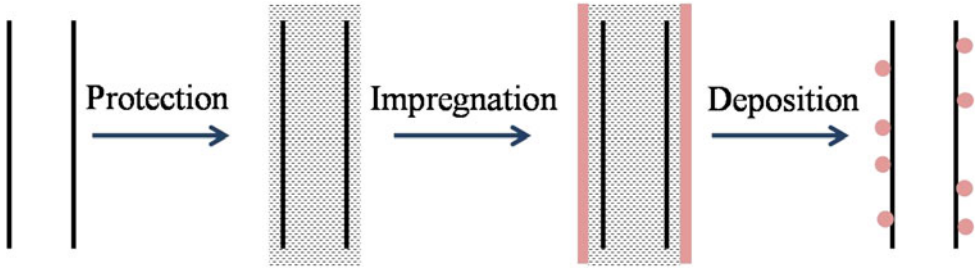

Fig. 6 Schematic view of the selective deposition of nanoparticles outside HNTs

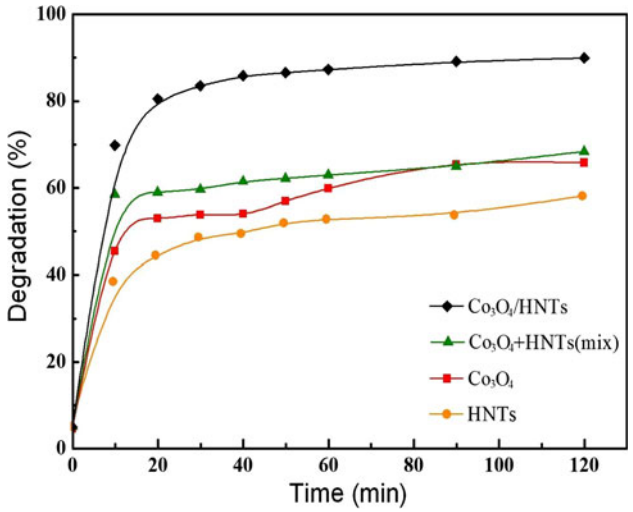

Fig. 7 Degradation of MB with Co_3O_4/HNTs, Co_3O_4+HNTs(mix), Co_3O_4 and HNTs

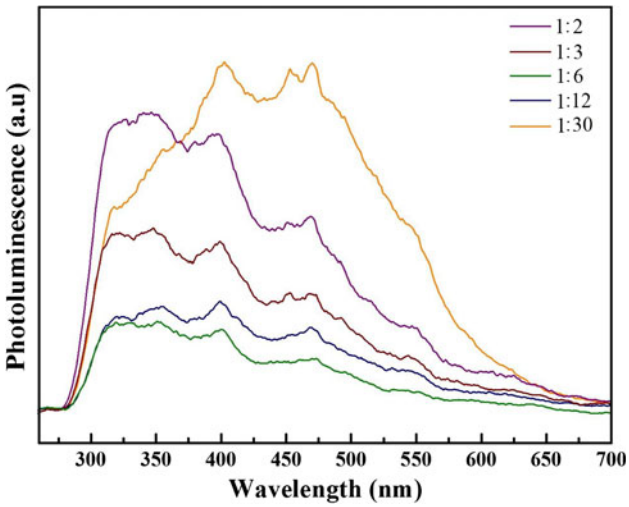

Fig. 9 PL spectra of the samples with different Co_3O_4/HNTs mass ratio

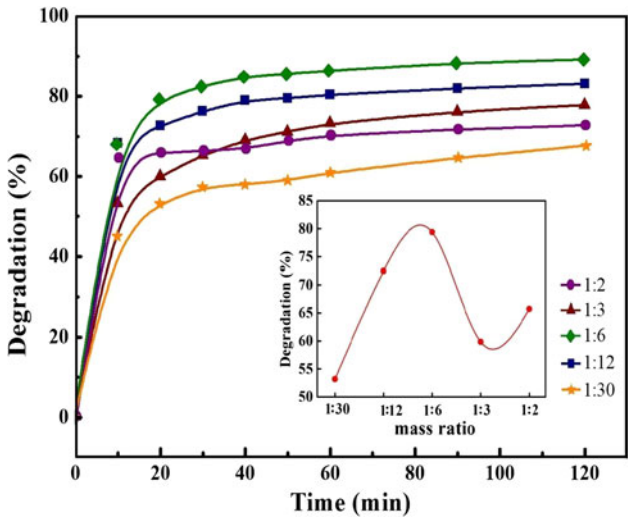

Fig. 8 Degradation of MB with the different Co_3O_4/HNTs mass ratio

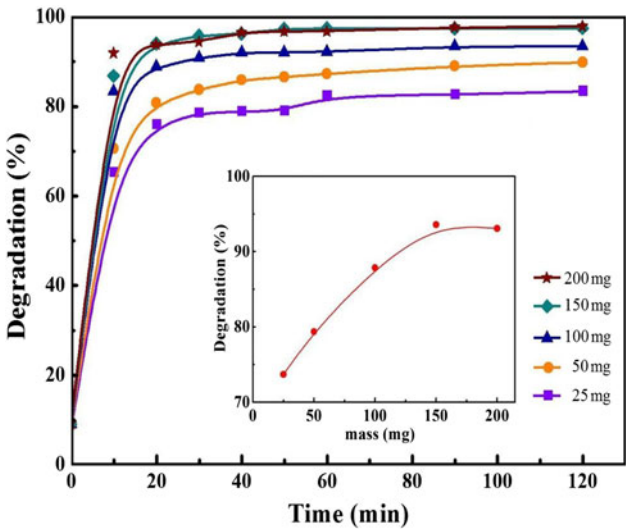

Fig. 10 Degradation of MB with the different amount of Co_3O_4/HNTs (1:6 sample)

absorption of 50 % of MB. Compared with the other samples, the efficiency of Co_3O_4/HNTs could reach as high as 79 % in 20 min and above 90 % in 2 h. In the photocatalytic process, halloysite was used as clay stabilizer to prevent the aggregation of Co_3O_4 and to enhance their photocatalytic. Co_3O_4 dispersed on the outer surface of HNTs would be more active than that on the inner surface because there was no photocatalysis activity when Co_3O_4 was dispersed on the inner surface. Figure 8 gave the experimental results of MB degradation at different Co_3O_4/HNTs mass ratio. Actually, the Co_3O_4/HNTs had an

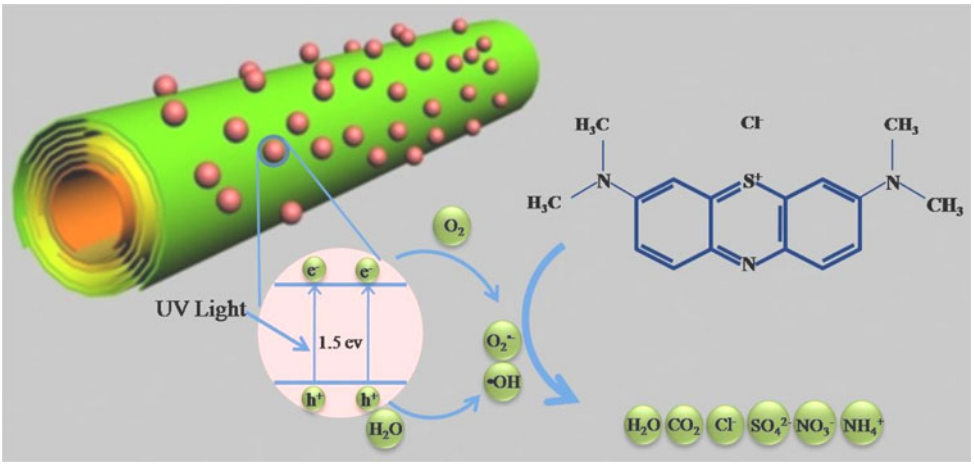

Fig. 11 Proposed mechanism of photocatalytic activity enhancement

excellent degradation (90 %) at Co_3O_4/HNTs mass ratio of 1:6, better than the others. The differences in photocatalytic activities between Co_3O_4/HNTs composite and other samples could be owing to the differences of their light absorption properties. Effective separation of the photogenerated charge carriers was acknowledged to be an important role on the high photocatalytic activity. So the room-temperature PL technique was employed to investigate the migration, transfer and recombination processes of the photogenerated electron–hole pairs on the as-synthesized samples (Chen et al. 2012). The lower the PL intensity, the higher the efficiency in photogenerated electron–hole separation, thus the higher photocatalytic activity. As shown in Fig. 9, the Co_3O_4/HNTs composite with 1:6 mass ratio sample showed the lowest PL peak intensity.

The effect of Co_3O_4/HNTs (1:6 sample) amount on the photocatalytic activity to the MB degradation was shown in Fig. 10, clearly indicating that the photocatalytic activity of Co_3O_4/HNTs could reach max 97 % at the Co_3O_4/HNTs amount of 150 mg. The UV irradiation (hv) activated Co_3O_4 to generate yield electrons (e) and holes (h), the yielded electrons (e) then reacted with the dissolved oxygen to produce superoxide anion radicals, while the holes were scavenged by the adsorbed water to form hydroxyl radicals (Pauporté et al. 2005). Finally, the active species (holes, superoxide anion radical or hydroxyl radical) oxidized the MB molecules adsorbed on the active sites of the Co_3O_4/HNTs system to enhance the photodegradation (Fig. 11). The whole photocatalytic reaction could be described as following:

$$Co_3O_4 + hv \rightarrow Co_3O_4 + (h + e) \quad (1)$$

$$Co_3O_4(e) + O_2 \rightarrow Co_3O_4 + O_2^{\cdot -} \quad (2)$$

$$Co_3O_4(h) + OH^- \rightarrow Co_3O_4 + \cdot OH \quad (3)$$

$$Co_3O_4(h) + \cdot OH + O_2^{\cdot -} + MB \rightarrow CO_2 + H_2O + SO_4^{2-} + NO_3^- + Cl^- \quad (4)$$

Conclusions

Co_3O_4 nanoparticles were successfully supported onto HNTs to prepare Co_3O_4/HNTs nanocomposites via incipient wetness impregnation method. The Co_3O_4/HNTs showed higher photodegradation activity to methyl blue than Co_3O_4+HNTs(mix), HNTs and pure Co_3O_4 nanoparticles. Particularly, the nanocomposites reached a high degradation of 97 %. The combination of the photocatalytic property of Co_3O_4 and the adsorptivity of HNTs endowed the as-prepared material with a bright perspective in environmental field.

Acknowledgments This work was supported by the National Natural Science Foundation of China (50774095) and the Scientific Research Foundation for ROCS of SEM (2011-1139).

References

Abdullayev E, Price R, Shchukin D, Lvov Y (2009) Halloysite tubes as nanocontainers for anticorrosion coating with benzotriazole. ACS Appl Mater Interfaces 1:1437–1443

Artero V, Chavarot-Kerlidou M, Fontecave M (2011) Splitting water with cobalt. Angew Chem Int Ed 50:7238–7266

Azadi P, Farnood R, Meier E (2010) Preparation of multiwalled carbon nanotube-supported nickel catalysts using incipient wetness method. J Phys Chem A 114:3962–3968

Cao AM, Hu JS, Liang HP, Song WG, Wan LJ, He XL, Gao XG, Xia SH (2006) Hierarchically structured cobalt oxide (Co_3O_4) the morphology control and its potential in sensors. J Phys Chem B 110:15858–15863

Casas-Cabanas M, Binotto G, Larcher D, Lecup A, Giordani V, Tarascon J (2009) Defect chemistry and catalytic activity of nanosized Co_3O_4. Chem Mater 174:1939–1947

Chen L, Yin S-F, Huang R, Zhang Q, Luo SL, Au CT (2012) Hollow peanut-like m-$BiVO_4$: facile synthesis and solar-light-induced photocatalytic property. CrystEngComm 14:4217–4222

Delannoy L, El Hassan N, Musi A, Le To NN, Krafft J-M, Louis C (2006) Preparation of supported gold nanoparticles by a modified incipient wetness impregnation method. J Phys Chem B 110:22471–22478

Du ML, Guo BC, Jia DM (2010) Newly emerging applications of halloysite nanotubes: a review. Polym Int 59:574–582

Endo M, Strano MS, Ajayan PM (2008) Potential applications of carbon nanotubes. Carbon Nanotubes 111:13–62

Gualtieri AF (2001) Synthesis of sodium zeolites from a natural halloysite. Phys Chem Miner 28:719–728

Guimarães L, Enyashin AN, Seifert G, Duarte HA (2010) Structural, electronic, and mechanical properties of single-walled halloysite nanotube models. J Phys Chem C 114:11358–11363

Hu PW, Yang HM (2012) Sb-SnO_2 nanoparticles onto kaolinite rods: assembling process and interfacial investigation. Phys Chem Miner 39:339–349

Hu LH, Peng Q, Li YD (2008) Selective synthesis of Co_3O_4 nanocrystal with different shape and crystal plane effect on catalytic property for methane combustion. J Am Chem Soc 130:16136–16137

Hughes AD, King MR (2010) Use of naturally occurring halloysite nanotubes for enhanced capture of flowing cells. Langmuir 26:12155–12164

Jiao F, Frei H (2009) Nanostructured cobalt oxide clusters in mesoporous silica as efficient oxygen-evolving catalysts. Angew Chem Int Ed 48:1841–1844

Joussein E, Pettit S, Churchman J, Theng B, Righi D, Delvaux B (2005) Halloysite clay minerals a review. Clay Miner 40:383–426

Levis SR, Deasy PB (2002) Characterisation of halloysite for use as a microtubular drug delivery system. Int J Pharm 243:125–134

Li W, Jung H, Hoa ND, Kim D, Hong S-K, Kim H (2010) Nanocomposite of cobalt oxide nanocrystals and single-walled carbon nanotubes for a gas sensor application. Sens Actuators B Chem 150:160–166

Liang YY, Li YG, Wang HL, Zhou JG, Wang J, Regier T, Dai HJ (2011) Co_3O_4 nanocrystals on graphene as a synergistic catalyst for oxygen reduction reaction. Nat Mater 10:780–786

Liu B, Aydil ES (2009) Growth of oriented single-crystalline rutile TiO_2 nanorods on transparent conducting substrates for dye-sensitized solar cells. J Am Chem Soc 131:3985–3990

Lvov YM, Shchukin DG, Möhwald H, Price RR (2008) Halloysite clay nanotubes for controlled release of protective agents. ACS Nano 2:814–820

Natile MM, Glisenti A (2002) Study of surface reactivity of cobalt oxides interaction with methanol. Langmuir 14:3090–3099

Pauporté T, Mendoza L, Cassir M, Bernard MC, Chivot J (2005) Direct low-temperature deposition of crystallized CoOOH films by potentiostatic electrolysis. J Electrochem Soc 152:C49–C53

Shchukin DG, Lamaka SV, Yasakau KA, Zheludkevich ML, Ferreira MGS, Mohwald H (2008) Active anticorrosion coatings with halloysite nanocontainers. J Phys Chem C 112:958–964

Takada S, Fujii M, Kohiki S (2001) Intraparticle magnetic properties of Co_3O_4 nanocrystals. Nano Lett 1:379–382

Veerabadran NG, Mongayt D, Torchilin V, Price RR, Lvov YM (2009) Organized shells on clay nanotubes for controlled release of macromolecules. Macromol Rapid Commun 30:99–103

Wang L, Chen J, Ge L, Zhu Z, Rudolph V (2011) Halloysite-nanotube-supported ru nanoparticles for ammonia catalytic decomposition to produce CO_x-free hydrogen. Energy Fuels 25:3408–3416

Woan K, Pyrgiotakis G, Sigmund W (2009) Photocatalytic carbon-nanotube-TiO_2 composites. Adv Mater 21:2233–2239

Wöllenstein J, Burgmair M, Plescher G, Sulima T, Hildenbrand J, Böttner H, Eisele I (2003) Cobalt oxide based gas sensors on silicon substrate for operation at low temperatures. Sens Actuators B Chem 93:442–448

Yeo BS, Bell AT (2011) Enhanced activity of gold-supported cobalt oxide for the electrochemical evolution of oxygen. J Am Chem Soc 133:5587–5593

Zhai R, Zhang B, Liu L, Xie YD, Zhang HQ, Liu JD (2010) Immobilization of enzyme biocatalyst on natural halloysite nanotubes. Catal Commun 12:259–263

Zhang Y, Yang HM (2012) Halloysite nanotubes coated with magnetic nanoparticles. Appl Clay Sci 56:97–102